D2.4 Optimized design for the closed loop geothermal system

Deliverable No.: D2.4

Deliverable lead: IFE

Authors: V. Leontidis, N. Anand, M. Wangen

Dissemination level: Public

Submission date: 19.12.2023

Funded by the European Union. Views and opinions expressed are however those of the author(s) only and do not necessarily reflect those of the European Union or CINEA. Neither the European Union nor the granting authority can be held responsible for them.

PROJECT INFORMATION

PROJECT ACRONYM	HOCLOOP
Call ID	HORIZON- CL5-2021-D3-03-15
Project title	A circular by design environmentally friendly geothermal energy solution based on a horizontal closed loop - HOCLOOP
Grant Agreement No	101083558
Start of Project	01.10.2022
Project Duration	42 Months
Type of Action	HORIZON Research and Innovation Actions
Coordinator	IFE

DOCUMENT INFORMATION

Deliverable No.	D2.4
Work Package	WP2
Deliverable Lead	IFE
Deliverable Authors	V. Leontidis (IFPEN), N. Anand (VITO), M. Wangen (IFE)
Issue	1/1
Due date	31.12.2023
Submission date	19.12.2023
Dissemination level[1]	PU
Nature[2]	R
Copyright	© 2023 Consortium

[1] Dissemination level: **PU** = Public, **SEN** = Sensitive, **R-UE/EU-R** = EU classified, **C-UE/EU-C** = EU classified, **S-UE/EU-S** – EU classified

[2] Nature of the deliverable: deliverable: **R** = Document, report; **DEM** – Demonstrator, pilot, prototype; **DEC** – Websites, patent, filings, videos etc; **DATA** – data sets, microdata, etc; **DMP** – Data Management Plan; **ETHICS**; **SECURITY**; **OTHER**

This project has received funding from the European Union's Horizon Europe research and innovation program under grant agreement No 101083558

DOCUMENT HISTORY

DATE	VERSION	MODIFIED BY	COMMENT
30.11.2023	0.1	V. Leontidis (IFPEN), N. Anand (VITO), J. Van Bael (VITO), M. Wangen (IFE), V. Harcouët-Menou (VITO), O. Vestavik (RW)	First draft for internal revision
01.12.2023	0.2	Mario Silva (IFE)	First internal revision
01.12.2023	0.3	Mario Silva (IFE)	Distributed for peer review
17.12.2023	0.4	Ola Vestavik (RW), Domenico Liotta (UNIBA)	Reviewer's comments
19.12.2023	1.0	V. Leontidis (IFPEN), Mario Silva (IFE)	Review addressed
19.12.2023	2.0	Mario Silva (IFE)	Final version

This project has received funding from the European Union's Horizon Europe research and innovation program under grant agreement No 101083558

TABLE OF CONTENT

LIST OF TABLES

This project has received funding from the European Union's Horizon Europe research and innovation program under grant agreement No 101083558

LIST OF FIGURES

This project has received funding from the European Union's Horizon Europe research and innovation program under grant agreement No 101083558

LIST OF ABBREVATIONS

ACRONYM	DESCRIPTION
BHE	Borehole Heat Exchanger
CFD	Computational Fluid Dynamics
GWellFM	Geothermal Well Flow Simulator
GTW	Geo-Thermal-Well
RANS	Reynolds Averaged Navier-Stokes
SST	Shear-Stress Turbulence
SWP	Streamwise Periodic
WP	Work Package

This project has received funding from the European Union's Horizon Europe research and innovation program under grant agreement No 101083558

EXECUTIVE SUMMARY

Scope of the deliverable

The objective of WP2 is to develop tools and models to predict the heat flow towards a closed-loop geothermal well and the associated temperature decrease of the surrounding rock, considering the rock properties, groundwater flow and the different layers of the walls of the well, such as casing and cement. Within WP2, Tasks 2.2 & 2.3 aim at integrating the available in-house models for the heat flow towards geothermal well from Task 2.1 in models for the heat and fluid flow in the annulus and the central pipe. The objective is to simulate different well configurations using water as pipe-fluid and test the heat transfer coefficients that control the heat flow from the well-wall interface to the fluid.

Various configurations have been investigated through 1D to 3D simulations, considering the thickness, the materials, the possibility of inserting some innovative geometries or even to create some small portion of vacuum. The simulations will also test different well-radii, bottomhole depths, rock heat conductivities and isolators between the inner pipe and the annulus. A specific configuration case has been further modelled by shape optimisation methods developed by VITO for the water case.

Main conclusions

A parametric study performed, using the in-house codes, over a range of geometrical characteristics, operational conditions and geological settings showed that the mass flow rate, the depth of the well and the geothermal gradient have the strongest impact, at least over the range of the tested values. The presence of any fluid (mud, water, oil-based) in the annulus part of the well completion slightly deteriorates the performance of the process, in terms of outlet temperature and power production.

The effect of eccentricity on the thermo-hydraulic performance of the pipe-in-pipe arrangement of the HOCLOOP concept was studied by CFD simulations using a RANS solver in conjunction with streamwise periodic flow assumptions. The results showed that the Nusselt number decreases drastically with increase in eccentricity and the friction factor decreases with increase in eccentricity. The first observation has a negative effect on system's performance by minimizing the power production, whereas the second finding has a positive effect by decreasing the power demands for circulating the fluid.

The impact of the Nusselt number on system's performance was studied in more details with GWellFM simulator. The results show that the decrease in Nusselt number has a low impact on the power production, visible mainly during the initial production period.

1. Introduction

To study the impact of different parameters on the performance of the closed loop solution proposed in the HOCLOOP project detailed simulations must be performed. It is, thus, important to consider in the numerical tests a realistic well configuration. A schematic representation of the well with the different

This project has received funding from the European Union's Horizon Europe research and innovation program under grant agreement No 101083558

layers is presented in Figure 1 by its cross-section.

The well generally consists of an external casing and two inner tubes. Between the inner tubes a layer of insulation material is placed. The fluid is injected at the surface in the space between the casing and the second inner tube, whereas it returns to the surface through the first inner tube. The diameters of the vertical and the horizontal wellbore aren't the same, because a smaller drilling bit is used to open the horizontal section. These values are detailed in Table 1 for both wellbore sections.

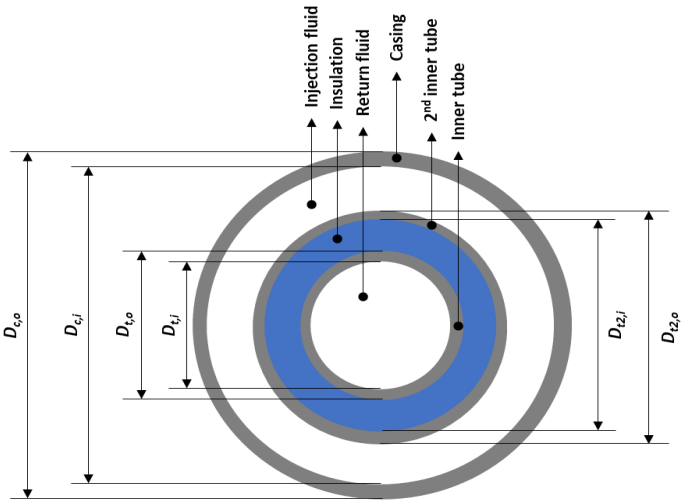

Figure 1. Representation of the cross-section of the well completion with the different layers .

Table 1. Geometric characteristics of the reference well completion for the vertical and horizontal sections.

Parameter	Vertical section	Horizontal section
Tube inner diameter, $D_{t,i}$ (mm)	85	85
Tube outer diameter, $D_{t,o}$ (mm)	101	101
2nd tube inner diameter, $D_{t2,i}$ (mm)	122	122
2nd tube outer diameter, $D_{t2,o}$ (mm)	140	140
Casing inner diameter, $D_{c,i}$ (mm)	253	273
Casing outer diameter, $D_{c,o}$ (mm)	194	175

In this report, initially the optimization results obtained from 3 in-house codes (GTW by IFE, GWellFM by IFPEN and BHEModel by UNIFI), which were previously benchmarked [1, 2], are presented for several well configurations and geological conditions. Then, a 3D flow simulation tool is applied for a specific well configuration to study the impact of the eccentricity of the inner tube in relation to the casing along the horizontal section on the performance of the system. This tool is based on two open-source software, the *SU2* multiphysics simulation tool, and the *Gmsh* 3D finite element mesh generator combined with an in-

This project has received funding from the European Union's Horizon Europe research and innovation program under grant agreement No 101083558

house code.

2. Optimization

A reference case that corresponds to a realistic well configuration was initially constructed. Then, several input conditions, geometric parameters and geological conditions were chosen as parameters to be modified for the sensitivity study. The objective was to cover a range of different operational conditions and geological settings where the closed loop solution could be integrated.

Table 2 summarizes the selected parameters and their range. The reference case has been highlighted in red.

As shown previously [2], the three simulators produce identical results when the same case is simulated. Thus, the simulations included in Table 2 were shared among the three institutes according to Table 3. However, for comparison reasons, the reference case was simulated by all the three codes .

Table 2. Range of the parameters for the parametric study .

Injection		Geometry		Insulation		Casing diameter				Rocks		
						Vertical		Horizontal		Gradient g_T (°C/km)	Conductivity k (W/m/K)	
Flow rate m (kg/s)	Injection temperature T_{inj} (°C)	Depth D (km)	Horizontal length L (m)	Conductivity k (W/m/K)	Thickness e (mm)	$D_{c,o}$ (mm)	$D_{c,o}$ (mm)	$D_{c,i}$ (mm)	$D_{c,i}$ (mm)		Vertical	Horizontal
5*	25	2	3	0.01	5	248	217	178	159	20	1.4	2
7.5	30	3	5	0.1	10.5	273	253	194	172	30	2	3
10	35	4	7	1	15	298	271	219	201	40	3	5

* The red values correspond to the reference case

Table 3. Applied wellbore models.

Parameter	Institute	Code	Type of transient model	More details
Reference, flow rate, depth, horizontal length	IFE	GTW	Numerical	[1, 2]
Reference, injection temperature, insulation material, gradient	UNIFI	BHEModel	Analytical	[2]
Reference, insulation thickness, casing diameter, rocks conductivity	IFPEN	GWellFM	Numerical	[1, 2]

This project has received funding from the European Union's Horizon Europe research and innovation program under grant agreement No 101083558

GTW and BHEModel codes cannot consider multiple layers between the injected and the returned fluid, i.e., two casings and an insulation layer in Figure 1. To overcome this limitation an average thermal conductivity representing all the solid layers is calculated according to Eq. (1)It is applied in the two codes as one material with inner and outer diameter equal to the inner tube and outer 2nd tube diameter, respectively. On the other hand, GWellFM can easily handle multilayers. The corresponding value of the average conductivity for the reference case is 0.0264 W/m/K, instead of 0.01 W/m/K.

$$k_{aver} = \frac{\log\left(\frac{D_{t2,o}}{D_{t,i}}\right)}{\frac{\log\left(\frac{D_{t,o}}{D_{t,i}}\right)}{k_t} + \frac{\log\left(\frac{D_{t2,i}}{D_{t,o}}\right)}{k_{ins}} + \frac{\log\left(\frac{D_{t2,o}}{D_{t2,i}}\right)}{k_{t2}}} \quad (1)$$

2.1. Reference case

In Figure 2 the temperature of the returned fluid in the outlet of the well and the produced power are compared between the three codes for the reference case and over a period of 20 years. The overall trend of the temporal variation for three codes is similar. To evaluate the difference between them, the error difference, δ, is calculated as:

$$\delta\Phi = \frac{|\Phi_1 - \Phi_2|}{\Phi_1} 100 \quad (2)$$

where Φ is the temperature or the power, and the subscripts 1 and 2 correspond to two of the codes.

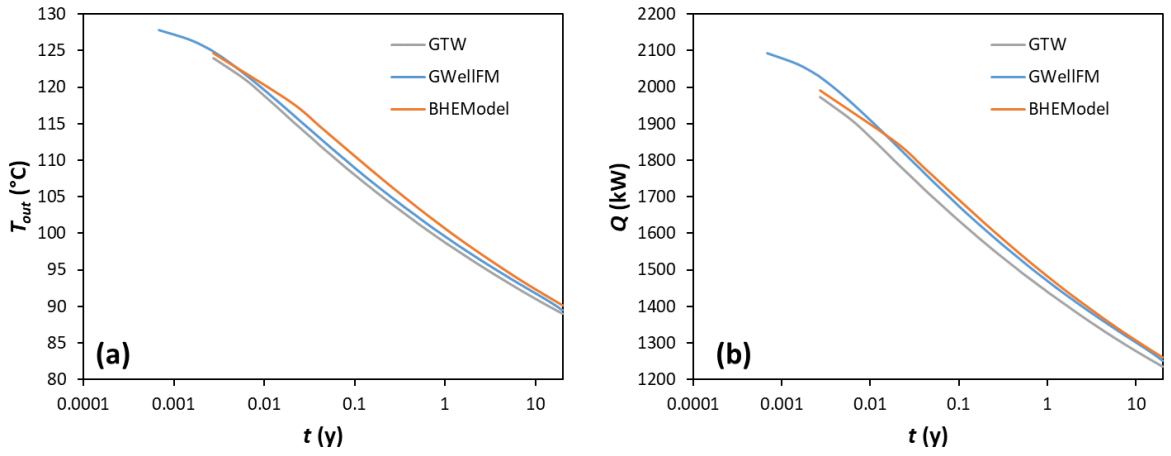

Figure 2. Comparison between GTW, GWellFM and BHEModel of (a) fluid's outlet fluid temperature and(b) power production for the reference case.

Table 4 summarizes the error when comparing GTW with GWellFM, GWellFM with BHEModel and GTW with BHEModel. The average error for the temperature prediction is less than 1.8% with GTW and BHEModel having the larger value and GWellFM / BHEModel the smallest. In all cases the highest error observed at the end of the simulated period. Similarly, the average error in the power prediction is around 2.8% between GTW / GWellFM and GTW / BHEModel, whereas only 1.2% between GWellFM and BHEModel.

This project has received funding from the European Union's Horizon Europe research and innovation program under grant agreement No 101083558

Table 4. Error (%) in the calculation of the outlet fluid temperature and power production between GTW, GWellFM and BHEModel for the reference case.

Time (d)	GTW / GWellFM		GWellFM / BHEModel		GTW / BHEModel	
	δT_{out}(%)	δQ(%)	δT_{out}(%)	δQ(%)	δT_{out}(%)	δQ(%)
1	0.668	2.824	0.203	1.833	0.463	0.940
7	0.754	2.649	1.214	0.362	1.978	3.021
30	0.860	2.558	1.463	0.962	2.336	3.545
90	0.815	2.382	1.385	1.033	2.211	3.439
365	0.789	2.153	1.118	0.852	1.915	3.022
1825	0.770	2.055	0.757	0.509	1.532	2.574
3650	1.766	3.488	0.347	1.089	1.412	2.361
7300	4.090	7.036	2.715	4.593	1.265	2.120
Average	**1.146**	**2.885**	**1.189**	**1.225**	**1.788**	**2.837**

2.2. Parametric study

For qualifying the impact of each parameter, the difference between the calculated value, Φ_{calc}, and the corresponding value of the reference, Φ_{ref}, of the parameter Φ (outlet temperature or the power production) is calculated, according to the equation:

$$\Delta\Phi = \Phi_{calc} - \Phi_{ref} \quad (3)$$

Values of the difference larger than zero mean that the increase (or the decrease) of the input parameter results in higher calculated values of the temperature or the power and thus the impact is characterised as positive, and negative for lower than zero differences values. The higher the difference, the stronger is the impact. Figure 3 and Figure 4 show the impact on the temperature and the power when decreasing and increasing the value of the input parameters, respectively.

It is obvious that with the decrease in the maximum temperature in the formation close to the horizontal section of the well both the outlet temperature and the power production decreases. This reflects situations where either the depth of the horizontal section or the geothermal gradient is decreased. Both these parameters have a strong impact on the efficiency of the closed-loop system.

Decreasing the length of the horizontal section or the rock conductivity around the horizontal part result in lower outlet temperature and energy production because the fluid recovers lower energy from the rocks. In the first case, the fluid remains in contact with hot rocks for a shorter overall period, whereas in the second, the heat transfer rate from the rocks towards the well is smaller. The impact of the length seems to be more important when decreasing the parameter rather than when increasing it, which may suggest that there is a specific length for getting the maximum out of the rocks and further increase of the length

This project has received funding from the European Union's Horizon Europe research and innovation program under grant agreement No 101083558

will have no impact since both the temperature and the power reach a plateau.

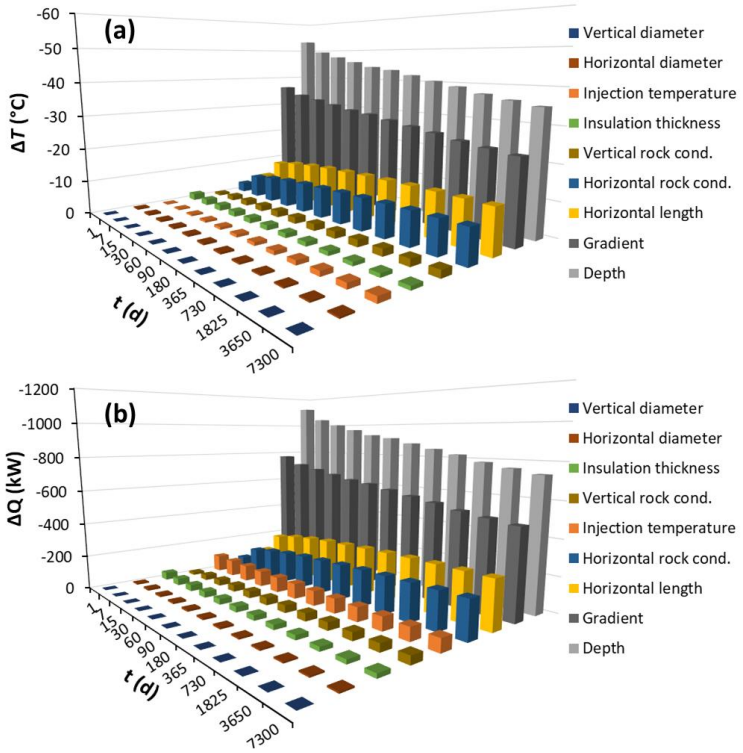

Figure 3. Impact on (a) the outlet temperature and (b) the power production of decreasing the values of the input parameters.

This project has received funding from the European Union's Horizon Europe research and innovation program under grant agreement No 101083558

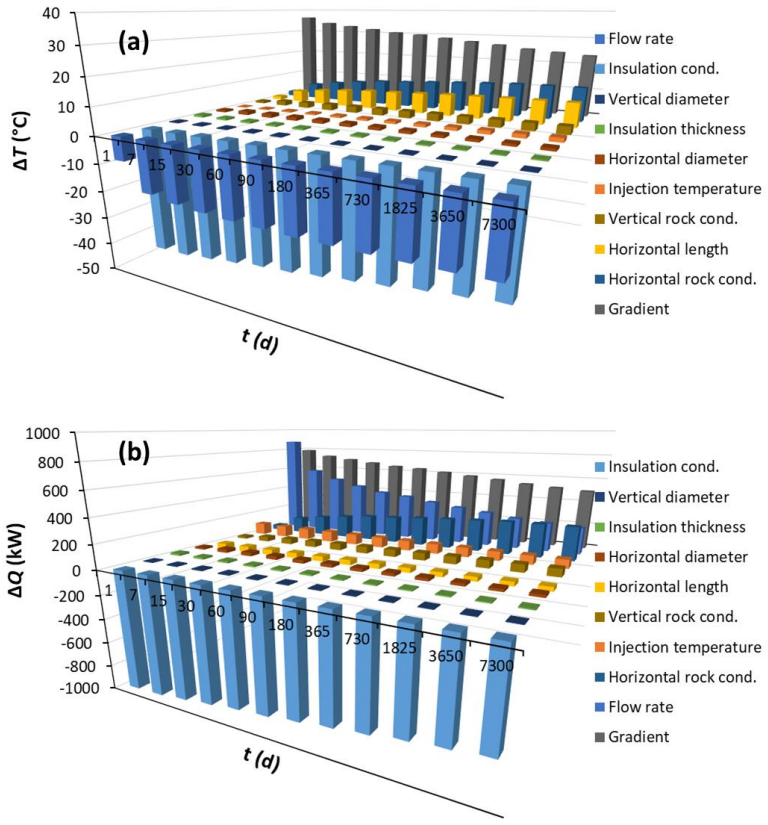

Figure 4. Impact on (a) the outlet temperature and (b) the power production of increasing the values of the input parameters.

The injection temperature, the vertical rock conductivity of the formation and the insulation thickness have a low impact, and the diameter of the casing both in the vertical and the horizontal sections have no practical impact, at least on the range tested in the study.

Increasing the thermal conductivity of the insulation material results in larger heat losses of the produced fluid, and thus lower power is produced. Finally, increasing the mass flow rate has negative impact on the outlet temperature but a strong positive impact on the power production. With higher flow rates, the fluid travels faster in the well staying less time in contact with the hot rocks and thus recovering less energy. However, the power output is higher because it is proportional to the mass rate according to the equation:

$$Q = m(H_{out} - H_{in}) \quad (4)$$

where H is the specific enthalpy in J/kg.

For quantifying the impact of each parameter on fluid's temperature and power production, Eq. (2) is applied to calculate the difference between each case and the reference case. When the difference is below 2% the impact of the parameter is characterised as low, above 10% as high and in between as moderate. Positive impact means that the increase in the value of a parameter results in higher outlet temperature or power. Table 5 summarizes the findings.

This project has received funding from the European Union's Horizon Europe research and innovation program under grant agreement No 101083558

Table 5.Summary of the impact of the increase of each input parameter on the outlet temperature and the power production.

Parameter	Impact	Outlet temperature	Power production
Flow rate	High	Negative	Positive
Injection temperature	Low	Positive	Negative
Depth	High	Positive	Positive
Horizontal length	Moderate	Positive	Positive
Insulation material	Moderate	Negative	Negative
Insulation thickness	Low	Positive	Positive
Vertical casing diameter	Low	Positive	Positive
Horizontal casing diameter	Low	Positive	Positive
Gradient	High	Positive	Positive
Vertical rocks conductivity	Low	Positive	Positive
Horizontal rocks conductivity	Moderate	Positive	Positive

2.3. Type of fluid in completion annulus

While drilling and installing the dual pipe a second annulus is formed between the casing and the rock (Figure 5). This section of the completion may be filled either with mud or with a fluid which is present in the reservoir during the drilling, which can be a water-based or an oil-based fluid. In addition, part of the annulus may be filled with one fluid (e.g., mud) and another part with another fluid (e.g., water- or oil-based).

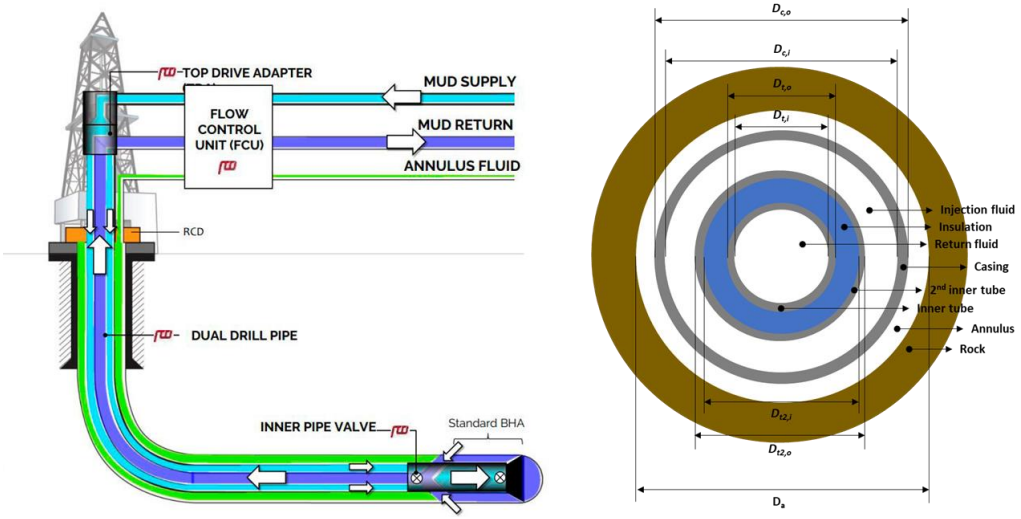

Figure 5.The complete closed loop well (left) and a cross section (left)

A series of simulations were performed using GWellFM to study the impact of the presence of this fluid. Again, the same reference case as previously is used for comparisons. The thickness of the annulus is set to 12.7 mm and the thermal conductivity of the fluids are given in Table 6. The results show that the higher

This project has received funding from the European Union's Horizon Europe research and innovation program under grant agreement No 101083558

is the thermal conductivity, the lower are the heat losses. In addition, the evolution of the outlet temperature and the power production is similar as in the reference case (without annulus side), as can be seen in Figure 6. The heat losses between the water-based and the oil-based fluid correspond to around 2 °C and 47 kW, whereas between water and mud they correspond to about 1 °C and 22 kW.

Table 6. Annulus' fluids and heat conductivities used.

Fluid	Conductivity (W/m/K)
Water-based	0.6
Oil-based	0.2
Mud	1.5

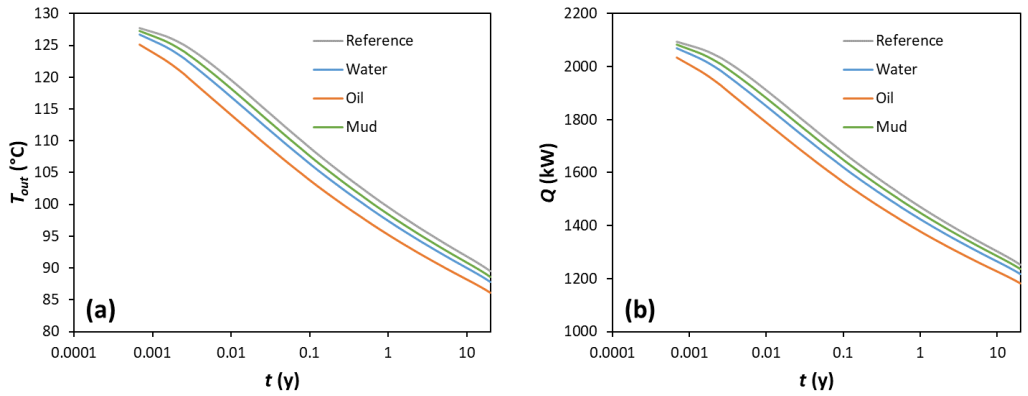

Figure 6. Impact on (a) the outlet temperature and (b) the power production by the presence of a fluid in the annulus part of the well completion.

In addition to the above simulations, additional cases were run for which the annulus section along the horizontal part was partially filled with mud and water or oil-based fluids. For a total of 5 km, the cases included in Table 7 were executed: L_1 is the length of horizontal section just after the vertical well and L_2 is the length of the last section. The annulus part in the vertical well is always full of mud.

Table 7. Distribution of two fluids in the annulus section of the horizontal part.

Fluid	L_1 (km)	L_2 (km)
Mud / water or oil-based	1	4
Mud / water or oil-based	2.5	2.5
Mud / water or oil-based	4	1

Figure 7 shows the temporal evolution of fluid's outlet temperature and power production when the annulus is partially filled with mud and water. The reference case (well without annulus) and the fully-filled with water have been included for comparison. Partially filled annulus results in slightly higher temperature and power when compared to the water case and in lower outcome when compared to the reference case.

This project has received funding from the European Union's Horizon Europe research and innovation program under grant agreement No 101083558

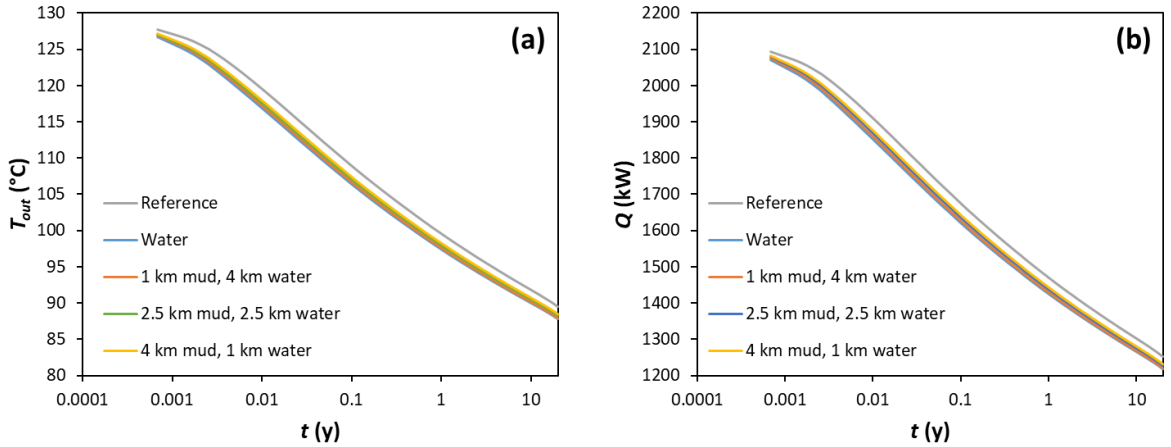

Figure 7.Horizontal annulus partially filled with mud and water: Temporal evolution of (a) the outlet temperature and (b) the power production.

3. Effect of eccentricity

The concentric pipe configurations of HOCLOOP concept are susceptible to many installation issues and one of them is the use of support structures to centre the return pipe inside the outer pipe. This is particularly difficult to achieve, primarily due to the difficulty in installation of these centring structures. As a result, considering the inner pipe to be concentric to the outer pipe is arguable.

In addition, all the thermal-hydraulic correlations available in the open literature limited to concentric pipes. As a result, the predicted performance of the geo-thermal plants is for concentric pipes (best case scenario) and does not take into the account the effect of the potential eccentricity of the pipes. Consequently, this leads to a huge uncertainty in the expected mal power output of geo-thermal plants with HOCLOOP concept. Hence, quantifying the effect of such eccentric arrangement of the inner pipe is critical to study the affect such pipe configuration might have on the performance of the geo-thermal power plant exploiting the HOCLOOP concept.

Stemming from these considerations, the objective of the research reported in this section is to quantify the deviation in the thermal and hydraulic performance due to eccentricity configuration of the pipes.

To achieve this, the concentric configurations of the pipe are first simulated using computational fluid dynamics (CFD). The obtained numerical results are benchmarked with the corresponding Nusselt Number (Nu) and friction factor coefficient (f) obtained from the Deliverable D2.1 [1] of the HOCLOOP project. This way the uncertainty between the correlations used in the project and those obtained from CFD can be quantified. Following this, numerical simulations are performed for the eccentric pipe configurations and the obtained deltas in the thermo-hydraulic performance are reported.

The flow is simulated by solving the Reynolds Averaged Navier-Stokes (RANS) equations [3], and the turbulence is modelled using the two equation Shear-Stress Turbulence (SST) model [4]. In addition, to reduce the computational cost of numerical simulations, a streamwise periodic flow assumption is made for the pipe channels. Thanks to the use of this streamwise periodic flow model [5], only a small section of the pipe can be simulated to predict the performance of a complete/full length pipe. The thermo-physical

This project has received funding from the European Union's Horizon Europe research and innovation program under grant agreement No 101083558

quantities are assumed to be constant in the flow domain.

3.1. Case f

The scope of this research is focused on case f of the HOCLOOP configuration, as reported in D2.1 [1]. In addition, to limit the number of simulations, the performance is evaluated only at the centre of the horizontal pipe at a steady-state condition after 10 years.

Case f is a horizontal coaxial closed loop well. It corresponds to a closed-loop system in a horizontal well as proposed in the HOCLOOP configuration. The inner pipe extends from the surface until the end of the horizontal well section (toe) as illustrated in Figure 5 in D 2.1 [1]. Here, the effect of heat leakage from the inner tubing to the annulus is captured and the comparison is made with Kabir's solution [6]. In deliverable D2.1 more details are given about the case f of the HOCLOOP configuration. For completeness, the full parameters list for case f is tabulated in Table 8.

3.2. Numerical setup

The flow in the passage was simulated using the incompressible RANS equations. The turbulence was modelled using the two equation SST model. Steady state solution was obtained by using a fixed-point iterator with a pseudo time stepping approach. To reduce the computation cost, streamwise periodic flow equation were solved, see Ref. [5]. The thermo-physical properties were assumed to be constant in the flow domain.

To simulate the flow in an annulus, a constant mass flow rate was specified as per the specification of case f, whereas the pressure drop per unit length is computed by iterations. To simulate flow conditions like that in the actual operation conditions, the outer surface of the outer pipe is specified with a constant heat flux value as obtained from case f. In addition, the inside of the annulus is specified with a heat flux value of 0 W/m^2 as the inner wall is insulated. More details about the boundary conditions used for the simulation can be found in Table 8 and Table 9. Figure 8 represents the computation flow domain with the specified boundary conditions.

Table 8: Parameters used as boundary conditions used for numerical simulation of case f.

No.	Parameter	Values	Units	Data source
1	Diameter outer (Casing inner)	0.1617	m	Table 9 [1]
2	Diameter inner (Insulation outer)	0.080	m	Table 9 [1]
3	Heat flux*	266.52 (after 10 years)	W/m^2	[7]
4	Temperature in Horizontal section	57.7 (after 10 years)	°C	[7]
5	Mass flow rate	8.8	kg/s	Table 10 [1]
6	Viscosity	0.0011	Pa.s	Table 8 [1]
7	Density	998.554	kg/m^3	Table 8 [1]
8	Pr (lam,turb)	7.867/1.9	-	Table 8 [1] & [8]

This project has received funding from the European Union's Horizon Europe research and innovation program under grant agreement No 101083558

*during numerical simulations heat flux values was increased by a factor of 1000 to remove catastrophic cancellation errors in numerical simulations

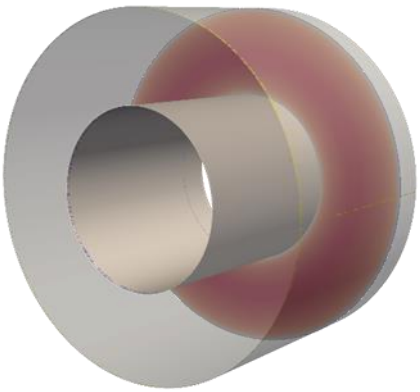

Figure 8. Illustration of flow domain of concentric pipe configuration.

Table 9. Type of CFD boundary condition used in the simulation.

Surface	Institute
Inflow	Periodic inflow (SWP)
Outflow	Periodic outflow (SWP)
Outer diameter	Heat flux = Specified
Inner diameter	Heat flux = 0 (insulated)

The current simulation framework does not include circumferential conduction of heat along the pipe. This can arguably have an impact on the overall heat-transfer in the pipe. However, to achieve this the current simulation framework needs to be extended. As a result, such analysis will be part of a future study.

3.3. Mesh convergence study

The mesh convergence study is an essential step to CFD-based numerical analysis to estimate the discretization error that might exist in the case under study. The mesh used in this study consist of a hybrid mesh, consisting of quadrilateral elements close to the wall and triangular elements in the area away from wall. The mesh used in this study was generated using the open-access code Gmsh [9].

To estimate this discretization error, three different meshes were numerically evaluated. They consisted of 262860, 1508019, 4421072 points in the mesh, hence forth referred to as coarse, fine and very-fine respectively. The two key indicators to study the discretization of the mesh was pressure drop (ΔP) and temperature difference (ΔT) between in inlet and outlet surfaces.

The results obtained from the mesh convergence study is illustrated in Figure 9 and the corresponding values are tabulated in Table 10. The results show that the fine mesh has a discretization error of 0.2% in terms of estimation of ΔP and 0.6% in terms of estimation of ΔT. Hence, based on these findings we can deem the fine mesh to be sufficient for the purpose of study of eccentricity.

This project has received funding from the European Union's Horizon Europe research and innovation program under grant agreement No 101083558

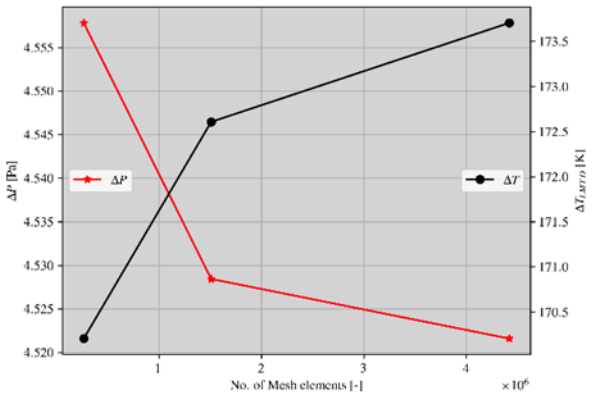

Figure 9. Mesh convergence study.

Table 10. Parameters from mesh convergence study.

Mesh	ΔP	%error	ΔT	%error
1	4.56	0.7%	170.21	1.4
2	4.53	0.2%	172.61	0.6%
3	4.52	-	173.71	-

For completeness, the mesh used for the study here onwards is reported in Figure 10.

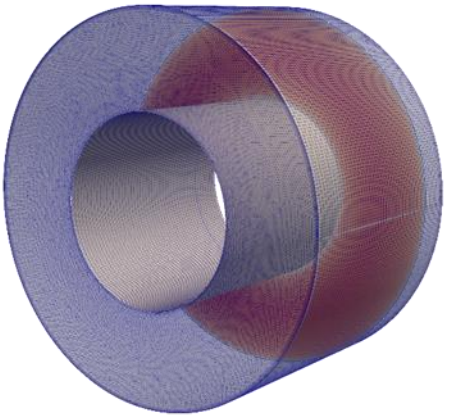

Figure 10. Representation of fine mesh used for the mesh convergence study.

3.4. Study of concentric pipes

To benchmark the CFD results with the correlations, the pipe simulation with concentric pipes were performed. The boundary conditions in this case remain identical to that elaborated in section Numerical setup and only the inner pipe is kept at the centre of the outer pipe, in other words they are concentric.

The state variables obtained from CFD simulations are used to obtain the Nu and f by using the following two equations:

This project has received funding from the European Union's Horizon Europe research and innovation program under grant agreement No 101083558

$$f_{CFD} = \frac{2\Delta P d_h}{\rho v^2 l} \quad (5)$$

$$Nu_{CFD} = \frac{h_{unit} l}{k} \quad (6)$$

The CFD results were compared with the Nu correlations used in deliverables D2.1 Eqs. (4)-(5) and to compare *f* Eqs. (8)-(10) of deliverable D2.2 [2] were used to estimate. Besides, correlations from open literature were also used to verify the numerical results. For this the Nu correlation were used as per [10] and friction factor was calculated using the VDI Heat Atlas [11].

Figure 11 shows the comparative results obtained for the concentric pipe case. It can be observed that the *f* obtained from CFD is 19% higher as compared to that used in the D2.2 [2] and the Nu is 1.3% higher as compared to that used in D 2.1 [1].

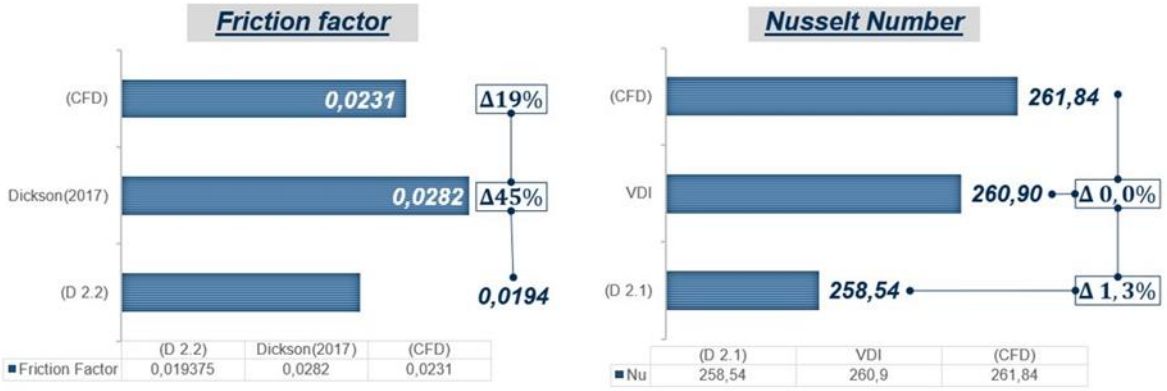

Figure 11. Parameters computed using CFD and the correlations. (left) friction factor (right) Nusselt Number.

Hence, it can be concluded that Nusselt numbers (*Nu*) obtained from CFD correlate well with that obtained from D2.1 [1], whereas *f* shows large deviations. Further study is recommended to understand the large variation in *f* used in the preliminary design of the plant.

3.5. Study on eccentricity

To study the eccentricity on the thermal-hydraulic performance of the coaxial pipe configurations, the inner pipe is offset from the centre, while maintaining the boundary layer thickness and discretization in the flow passage volume. The extend of eccentricity (C) is referred in term of percentage, wherein, C = 0% refers to concentric pipes (best condition) and C = 100% mean that the inner pipe is touching the bottom of the outer pipe (worst condition). Figure 12 illustrates the two extreme cases of the coaxial pipe, namely, C=0% and C=100%. To understand the effect of eccentricity on the thermo-hydraulic performance of the pipes, simulation for eccentric pipes was done in steps of 10% from 0% till 90%. The case with C=100% was not simulated due to the difficulty of solving the flow close to location where the two pipe surfaces touch each other.

This project has received funding from the European Union's Horizon Europe research and innovation program under grant agreement No 101083558

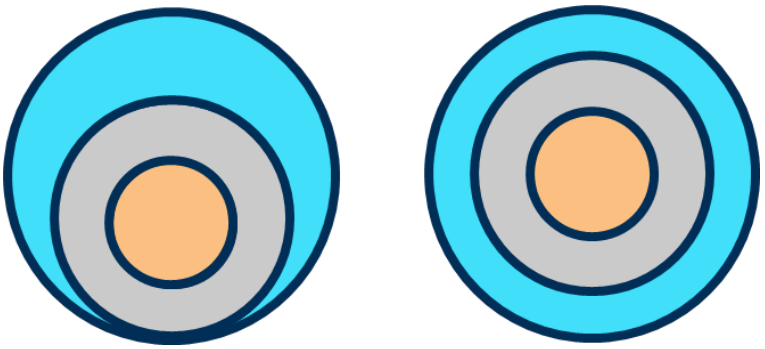

Figure 12. Illustration of extreme cases of eccentricity, left eccentricity C = 100% and right eccentricity C = 0%.

The boundary and the flow conditions used to simulate the effect of eccentricity are identical to that reported in section Numerical setup. The only variable is the value of C and the corresponding mesh configurations.

Figure 13, represent the velocity profile at the mid-section of the pipe. It can be observed that as the eccentricity increases from 10% to 90% the area of low velocity increases at the bottom of the outer pipe. In addition, it can be observed that the area of high velocity shift from the bottom of the inner pipe to the top of the inner tube.

In Figure 14, spider plot of the mass averaged flow properties is presented. The spider plots consist of (1) heat transfer coefficient (h), (2) area distribution, (3) ΔT_{LMTD} and (4) velocity magnitude. From the spider plots, it is observed that the local heat transfer coefficient at the bottom of the pipe, between 225° and 315°, reduces drastically when going from C of 60% to 90%. This change in local heat transfer coefficient can be attributed to the increase in the local ΔT_{LMTD}. In addition, the velocity magnitude is observed to be lower at the bottom of the pipes (or locations with smaller cross-sectional area) as compared to the coaxial case and vice-versa for locations with high area.

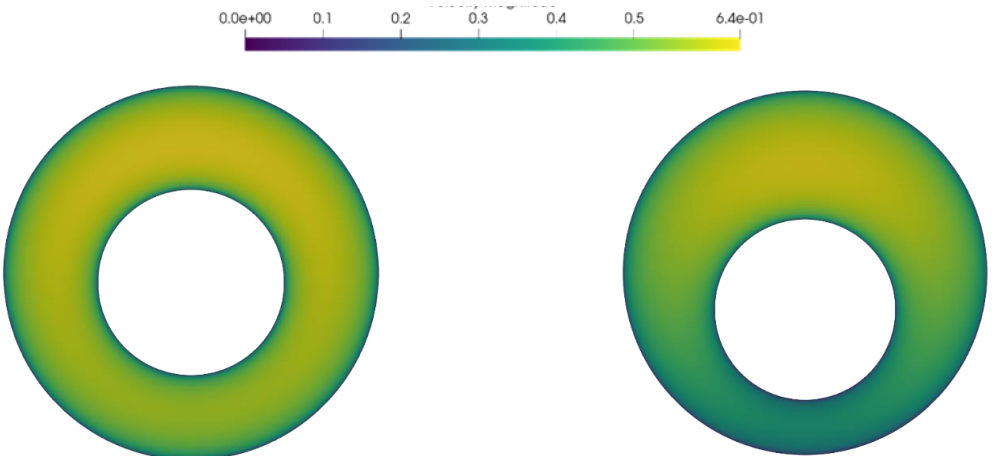

This project has received funding from the European Union's Horizon Europe research and innovation program under grant agreement No 101083558

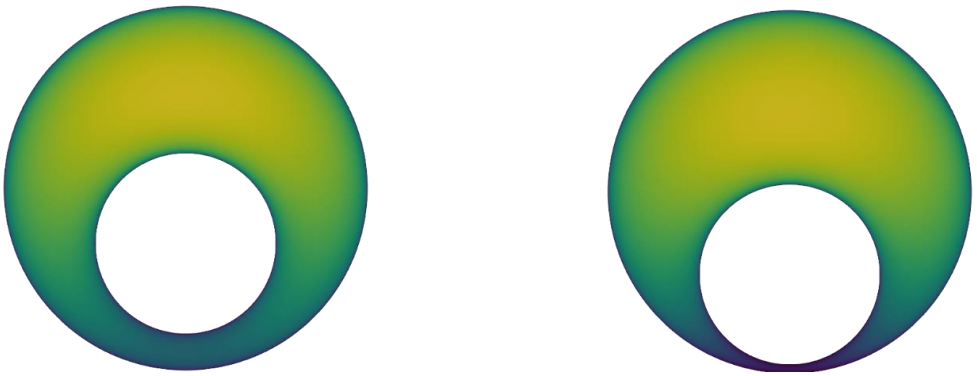

Figure 13: Variation of velocity field in the annulus cross-section with eccentricity; top-left C=10%, top-right C=40%, bottom-left C=80% and bottom-right C=90%.

Furthermore, Figure 15 illustrates the variation of friction factor coefficient and Nusselt Number with the eccentricity. It can be observed that the friction factor decreases by as much as 25% for C = 90% as compared to the eccentricity of 0%. Besides, it can also be observed that the Nusselt number decreases by more than 70% for C = 90% as compared to the baseline values for C = 0%.

From these observations, it can be concluded that although pressure drop reduces in the annulus with the increase in the eccentricity, the overall heat transfer coefficient reduces substantially which might affect the thermal effectiveness of the geothermal plant (Figure 16).

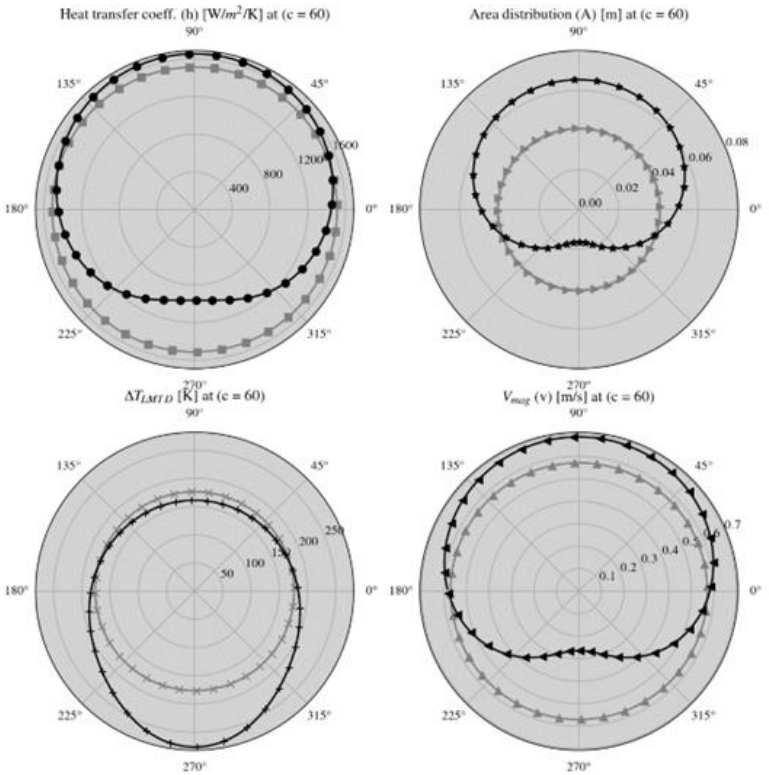

Figure 14. Spider plot illustrating the circumferential variation of properties for C = 60%; top-left heat transfer coefficient, top-right area distribution, bottom-left ΔT_{LMTD}, bottom-right V_{mag}. Grey lines represent values at C = 0%.

This project has received funding from the European Union's Horizon Europe research and innovation program under grant agreement No 101083558

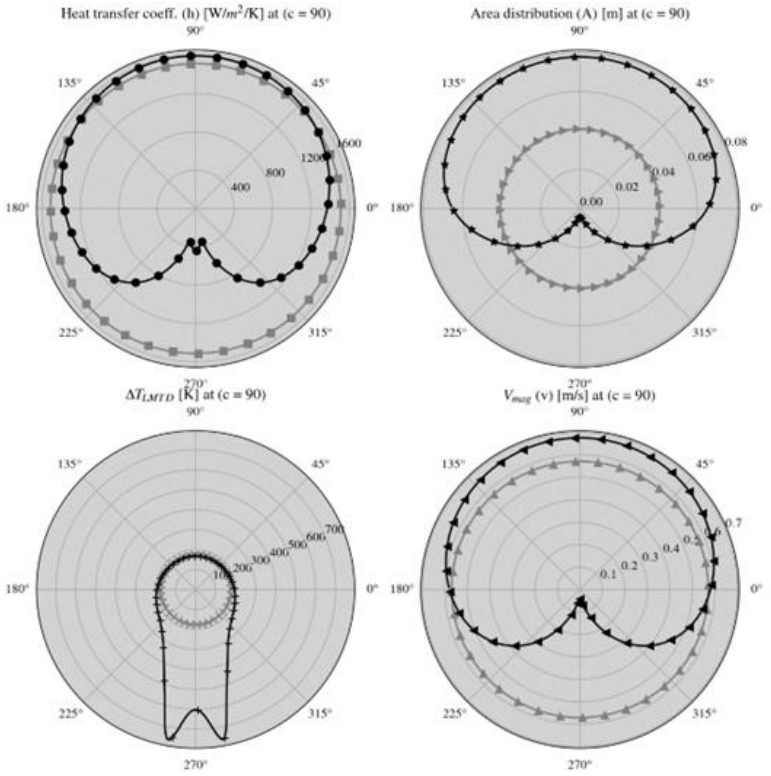

Figure 15. Spider plot illustrating the circumferential variation of properties for C = 90%; top-left heat transfer coefficient, top-right area distribution, bottom-left ΔT_{LMTD}, bottom-right V_{mag}. Grey lines represent values at C = 0%.

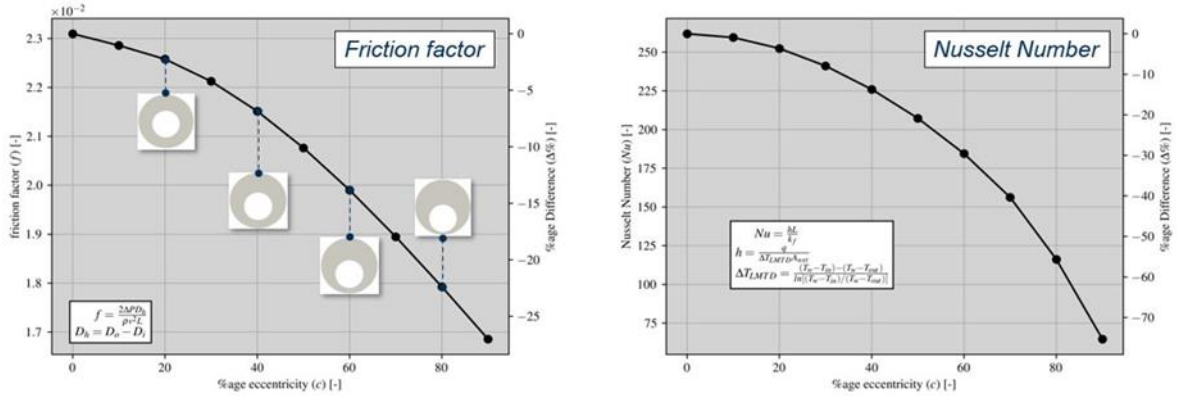

Figure 16. Variation of friction factor (left) and Nusselt Number (right) with C.

4. Impact of Nusselt number

Figure 16Table 11Figure 17Figure 18(2)To study the impact of the Nusselt number on the efficiency of the system, GWellFM was used to perform an additional set of simulations. In these simulations, the fixed *Nu* values reported in Table 11 were imposed. Note that the code had to be modified to consider a fixed Nu. Figure 17 shows the evolution of the outlet temperature and produced power for 10 years of operation of case f, whereas Figure 18 includes the difference, given by Eq. (2), between the reference case and the new

This project has received funding from the European Union's Horizon Europe research and innovation program under grant agreement No 101083558

calculated values.

Table 11. Variation of Nusselt number.

Case	Ref	1	2	3	4	5
Nusselt	262	230	190	150	110	70

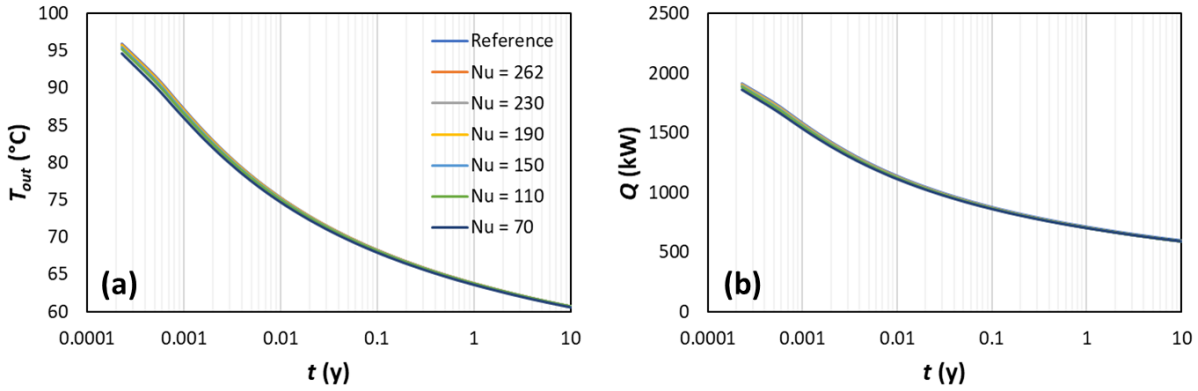

Figure 17. Impact of Nusselt number on (a) the outlet temperature and (b) the power production.

The impact of the Nusselt number on fluid's outlet temperature and power production is very low, with the maximum difference being around 1.5% for the lower Nusselt number. In addition, the difference always decreases with time. Lower Nusselt number means lower thermal convection, thus the fluid temperature is higher. However, in all cases the convection part in the heat losses is limited in comparison to the heat conduction, which is taking place with longer characteristic times and dominates.

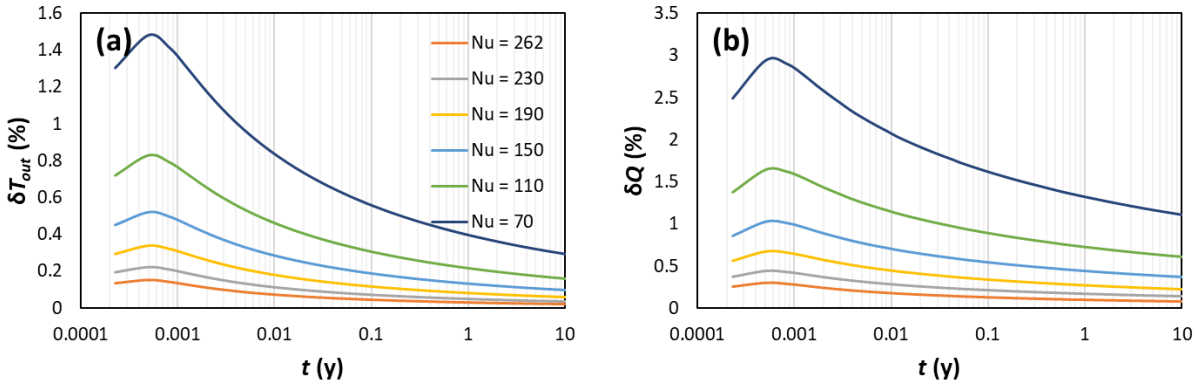

Figure 18. Difference (%) of (a) the outlet temperature and (b) the power production between the reference case and the cases with different Nusselt number.

This project has received funding from the European Union's Horizon Europe research and innovation program under grant agreement No 101083558

5. Conclusions

The parametric study performed for a realistic well configuration and geological settings showed that the mass flow rate, the depth of the well and the geothermal gradient have the strongest impact, while the length of the horizontal section, the insulation material and the rock conductivity have a moderate impact, at least over the range of the tested values. Considering the presence of a fluid (mud, water, oil-based) in the annulus part of the well completion resulted always in a performance of the process with slightly lower efficiency, in terms of outlet temperature and power production.

The effect of eccentricity on the thermo-hydraulic performance of the pipe-in-pipe arrangement of the HOCLOOP concept was studied by CFD simulations using a RANS solver in conjunction with streamwise periodic flow assumptions. The conclusions drawn from the scope of this work are:

- The mesh used for the numerical analysis consists of a discretization error of less than 1%.
- The Nusselt number and friction factor coefficient obtained from CFD showed a 1.3% and 19% variation, respectively, as compared to the values used from corelations reported in D2.1 [1] and D2.2 [2].
- The Nusselt number decreases drastically with increase in eccentricity. More specifically, the Nusselt number reduces by more than 70% when compared to its value for the concentric configuration.
- The friction factor decreases with increase in eccentricity. More specifically, the friction factor can decrease by as much as 25% when compared to its value for the concentric configuration.

The impact of the Nusselt number on the performance of the system was further studied using the GWellFM simulator. The simulations showed that the impact is generally low on power production, and it is limited on the early operation times.

6. References

[1] E. Acevedo, V. Leontidis, M. Wangen and V. Harcouët-Menou, "Benchmark cases D2.1," HOCLOOP Project 101083558, 2023.

[2] V. Leontidis, M. Wangen, P. Ungar and D. Fiaschi, "Flow pipe model for fluid circulation D2.2," HOCLOOP Project 101083558, 2023.

[3] T. D. Economon, F. Palacios, S. R. Copeland, T. W. Lukaczyk and J. J. Alonso, "SU2: An open-souce suite for multiphysics simulation and design," *AIAA Journal,* pp. 828-846, 2015.

[4] F. R. Menter, M. Kuntz and R. and Langtry, "Ten Years of Industrial Experience with the SST Turbulence Model," *Turbulence, Heat and Mass Transfer,* pp. 625-632, 2003.

[5] S. Patankar, C. Liu and E. M. Sparrow, "Fully developed flow and hear transfer in ducts having streamwise-periodic variations of cross-sectional area.," *Journal of Heat Transfer,* vol. 99, pp. 180-

This project has received funding from the European Union's Horizon Europe research and innovation program under grant agreement No 101083558

187, 1977.

[6] P. Sharma, A. Al Saedi and C. Kabir, "Geothermal energy extraction with wellbore heat exchanger: Analytical model and parameter evaluation to optimize heat recovery," *Renewable Energy,* vol. 166, pp. 1-8, 2020.

[7] E. Acevedo, *Personal communication,* VITO, June 2023.

[8] W. M. Kays, "Turbulent Prandtl Number - Where are we ?," *Journal of Heat Trasnfer,* vol. 116, no. 2, pp. 284-295, 1994.

[9] N. Schlomer, "pygmsh: A python front end for Gmsh," github, GPL-3.0, 2020.

[10] D. D. Ndenguma, J. Dirker and J. P. Meyer, "Heat transfer and pressure drop in annuli with approximately unifrom internal wall temperatures in the transtional flow regime.," *International Journal of Heat and Mass Transfer,* vol. 111, pp. 429-441, 2017.

[11] P. Stephan, H. Martin, S. Kabelac, D. Mewes, M. Kind and K. Schaber, VDI Heat Atlas, Second ed., Dusseldorf: Springer, 2010.

This project has received funding from the European Union's Horizon Europe research and innovation program under grant agreement No 101083558